ISIJ International, Vol. 48 (2008), No. 10, pp. 1380–1388

Heat Transfer in Funnel-mould Casting: Effect of Plate Thickness

Begoña SANTILLANA,[1)] Lance C. HIBBELER,[2)] Brian G. THOMAS,[2)] Arie HAMOEN,[1)] Arnoud KAMPERMAN[3)] and Willem VAN DER KNOOP[1)]

1) Corus RD&T SCC/CMF, P. O. Box 10000, 1970 CA IJmuiden, The Netherlands. E-mail: begona.santillana@corusgroup.com, arie.hamoen@corusgroup.com, willem.van-der-knoop@corusgroup.com 2) University of Illinois at Urbana-Champaign, Department of Mechanical Science and Engineering, 1206 West Green Street, Urbana, IL, USA 61801. E-mail: lhibbel2@uiuc.edu, bgthomas@uiuc.edu 3) Corus Strip Products IJmuiden/Direct Sheet Plant, P. O. Box 10000, 1970 CA IJmuiden, The Netherlands. E-mail: arnoud.kamperman@corusgroup.com

(*Received on April 24, 2008; accepted on July 9, 2008*)

Plant measurements and three-dimensional models are used to develop an accurate and efficient model of heat transfer in a thin-slab continuous casting mould, interface, and solidifying shell. A finite-element model of the complex-shaped mould, developed using ABAQUS, is applied to find offset correction factors that enable the efficient CON1D model to accurately predict temperature at thermocouple locations. Model interface parameters are calibrated using an extensive database of plant data obtained from the Corus Direct Sheet Plant in IJmuiden, The Netherlands, including measurements of mould heat removal, mould temperature, oscillation mark shape, mould-powder consumption, and mould thickness. The validated CON1D model is applied to quantify the combined effects of casting speed and mould plate thickness on mould heat transfer. Increasing casting speed causes a thinner solidified steel shell, higher heat flux, higher mould hot face temperature, a thinner slag layer and lower solid slag layer velocity. Increasing mould plate thickness increases hot face temperature, lowers solid slag layer velocity, increases slag layer thickness, and lowers mould heat flux.

KEY WORDS: thin-slab casting; funnel mould; heat transfer; mould thickness; numerical model; continuous casting.

1. Introduction

Mould heat transfer is important to mould life, surface quality, breakouts and many other aspects of the steel continuous-casting process. Heat transfer in funnel moulds has been investigated in only a few previous studies, examining heat flux profiles,[1)] mould distortion and cracking,[1–3)] phenomena in the steel/flux interface,[4–6)] and fluid flow coupled with solidification heat transfer.[7)] Heat flux tends to be higher in thin-slab casting than in conventional billet or slab casting, which is attributed to the higher casting speeds.[1)] Computational models can reveal insights into mould heat transfer, so long as they have been calibrated with plant data. Recent modelling studies of billet casting, which use thermocouple measurements and inverse heat transfer calculations to determine the heat flux profile, have shown that mould hot-face temperature increases with increasing mould plate thickness and casting speed.[8–10)] Another such model, CON1D,[11)] simulates one-dimensional heat transfer in the mould, interface, and solidifying shell,[6)] and has shown how interfacial slag properties affect heat transfer and lubrication.[5)]

In the present study, the CON1D model is applied to simulate high-speed thin-slab casting in a funnel mould. To account for the multidimensional thermal behaviour around the cooling channels of the funnel mould, a three-dimensional finite-element model, developed using ABAQUS 6.6-1,[12)] is applied to find correction factors that enable CON1D to predict accurately temperature at thermocouple locations. The model calculations have been validated using an extensive database of plant data obtained from the Corus Direct Sheet Plant (DSP) in IJmuiden, The Netherlands, including measurements of mould powder consumption, oscillation mark shape, mould temperature, and heat removal. The improved CON1D model is applied here to predict casting behaviour for different speeds and to investigate the effect of mould plate thickness. The results will be used to extrapolate standard practices to higher casting speeds and new mould designs.

2. CON1D Model Description

The heat transfer model CON1D simulates several aspects of the continuous casting process, including shell and mould temperatures, heat flux, interfacial microstructure and velocity, shrinkage estimates to predict taper, mould water temperature rise and convective heat transfer coefficient, interfacial friction, and many other phenomena. The heat transfer calculations are one-dimensional through the thickness of the shell and interfacial gap with two-dimensional conduction calculations performed in the mould. An entire simulation requires only a few seconds on a modern PC.

Heat transfer in the mould is computed assuming a slab

with attached rectangular blocks that form the cooling-water channels and act as heat transfer fins. The process parameters used in this analysis are typical values used with the Corus DSP thin-slab continuous-casting machine. Key parameters include a strand thickness of 90 mm, low carbon steel poured temperature of 1 545°C, and a meniscus level of 100 mm below the top of the 1 100 mm-long funnel mould. The casting speeds used in model calibration are 4.5 m/min for the narrow face and 5.2 m/min for the wide face. The different casting speeds were used to show that the correction factors depend only on mould geometry. To model accurately the complex geometry of the mould and water slots on both faces, geometry modifications and an offset methodology[13] are applied to calibrate the CON1D model to match the temperature predictions of a full three-dimensional finite element model created with ABAQUS.

2.1. Narrow Face

To create the simple mould geometry for CON1D, the actual narrow face cross-section was transformed into the one-dimensional rectangular channel geometry (dotted lines), as shown in **Fig. 1**. The bolt holes are 22 mm in diameter and 20.5 mm deep; the thermocouple holes are 4 mm in diameter and extend into the mould such that they are 20 mm beneath the hot face.

To approximate the actual geometry, the shortest distance between the water channels and the hot face was maintained at 24 mm and the pitch between the channels similarly was set to 12 mm. To match the water flow rate, the dimensions of the rectangular channels were chosen to keep the cross-sectional area nearly the same as that of the actual 14 mm diameter channels. In addition, to maintain heat transfer characteristics, the channel width was chosen to be about two-thirds of the diameter of the actual round channel. These two considerations yield a 9 mm by 17 mm channel and a 41 mm thick mould. CON1D aims only to model a typical section through the mould and cannot predict variations around the mould perimeter, such as corner and funnel effects.

2.2. Wide Face

Water channels in the wide face required similar dimensional adjustments for CON1D. The actual water channels are spaced 5 mm apart and are 5 mm wide by 15 mm deep with rounded roots.

The CON1D water channels are 5 mm wide but only 14 mm deep, so that filled area equals the hatched area in **Fig. 2**, and the cross sectional area again roughly equals that of the actual channel. The mould thickness was maintained at 35 mm. As shown in **Fig. 3**, this keeps the channels at a constant distance of 21 mm from the hot face, in comparison with the real mould, where the closest point of the rounded channel root is 20 mm from the hot face. The bolt holes have the same dimensions as on the narrow face, but on the wide face the thermocouple holes extend into the mould such that they are 15 mm from the hot face.

3. CON1D Model Offset Determination

To enable CON1D to accurately predict the thermocouple temperatures, it was calibrated using a three-dimensional heat transfer calculation to determine an offset distance for each mould face to adjust the modelled depth of the thermocouples.

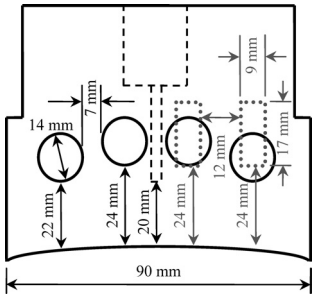

Fig. 1. Narrow face mould geometry and CON1D simplification.

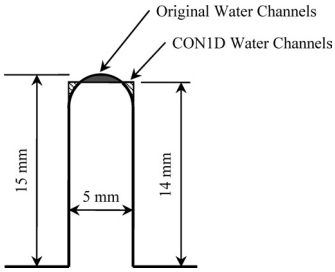

Fig. 2. Wide face water slot and CON1D simplification.

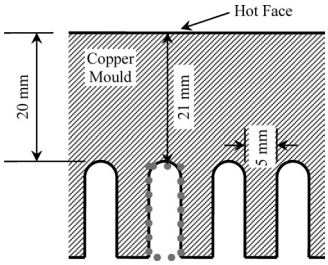

Fig. 3. Wide face mould geometry.

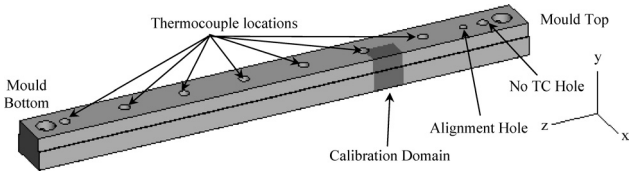

Fig. 4. Location of narrow face calibration domain.

3.1. Narrow Face

Two different three-dimensional heat transfer models were developed of the mould copper narrow faces (end plates) using ABAQUS. The first was a small, symmetric section of the mould geometry containing one quarter of a single thermocouple, which was used to determine the offset for CON1D. The second was a complete model of one symmetric half of the entire mould plate, used to determine an accurate temperature distribution including the effects of all geometric features and to evaluate the CON1D model.

To properly compare the finite-element model with CON1D, identical conditions were applied to both models. **Figure 4** shows the location of a typical repeating portion of the entire mould plate, and **Fig. 5**(a) shows the mesh and

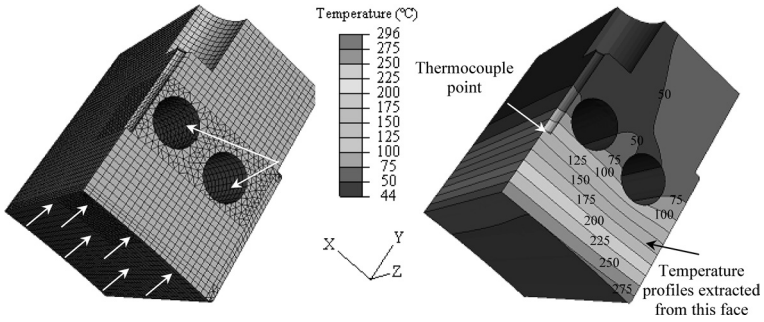

Fig. 5. Narrow face model, boundary conditions, and calibration results.

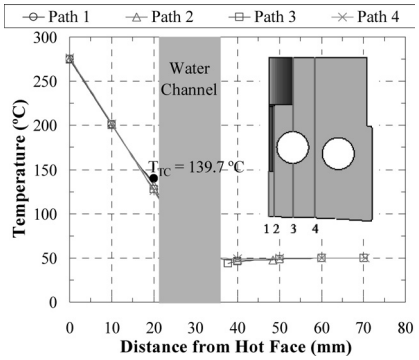

Fig. 6. Temperature profiles in narrow face.

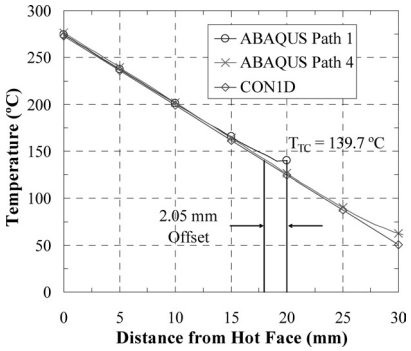

Fig. 7. Determination of offset.

simplified boundary conditions used for this calibration domain. The applied heat flux Q (2.6 MW/m^2) to the hot face is constant and uniform, as are the thermal conductivity k (350 W/(m·K)) of the mould, the convective heat transfer coefficient h (40 kW/(m^2·K)) and the water temperature T_∞ (36°C) applied to the water channel surfaces. Unlabelled surfaces are insulated (Q=0). The finite-element mesh used 45 840 hexahedron, tetrahedron and wedge quadratic elements and ran in 80 s (wall clock) on a 2.0 GHz Intel Core2 Duo PC.

Figure 5(b) shows the computed three-dimensional temperature contours and identifies the location of the thermocouple, as well as the face from which further data were extracted. The maximum temperature of 296°C is found on the hot face corner, which is 20.5°C hotter than the hot face centreline. The temperature profiles along four paths are shown in **Fig. 6**, in which a linear temperature gradient is evident between the hot face and the water channels. The temperature variation between these paths is small, with only 2°C difference across the hot face in the vicinity of the paths. The lowest temperature is found on the back (cold face side) of the water channel (Path 3). However, the missing copper around the thermocouple causes the local temperature to rise about 10°C. To account for this effect in CON1D, an offset distance is applied to the simulated depth of the thermocouples.

An offset distance enables the one-dimensional model to relate accurately thermocouple temperatures by accounting for three-dimensional conduction effects from the complex local geometry.[13] The difference in position between the thermocouples in the mould and in the model is called an "offset," which is the distance the thermocouple position is shifted when input to the CON1D model.

Figure 7 compares the temperature distribution of CON1D with the Path 1 results from Fig. 6. Although CON1D cannot capture the localized effects of the complex geometric features, the three-dimensional thermocouple temperature can be found by "moving" the thermocouple to a new location closer to the hot face. This small "offset distance," allows accurate thermocouple temperatures to be predicted by CON1D. The offset value can be determined from Eq. (1) using the CON1D temperature profile as follows:

$$d_{\text{offset}} = (T_{\text{TC}} - T_{\text{hf}})\frac{dx}{dT} - d_{\text{TC}}$$
$$= (139.7 - 273.16)^{\circ}\text{C} \cdot \frac{30\ \text{mm}}{(50.21 - 273.16)^{\circ}\text{C}} - 20\ \text{mm}$$
$$= 2.05\ \text{mm} \quad \text{.....(1)}$$

Where d_{offset}: the offset distance (mm)
T_{TC}: thermocouple temperature from ABAQUS (°C)
T_{hf}: the thermocouple temperature from CON1D (°C)
dx/dT: the inverse of the temperature gradient from CON1D (mm/°C)
d_{TC}: the actual depth of the thermocouple from the hot face (mm)

Figure 7 also shows that CON1D is able to match the three-dimensional results from the hot face to the water slot roots. Its accuracy drops in the non-linear water-slot portion of the mould, and near the thermocouple location, where matching is achieved by via the offset method.

3.2. Wide Face

Following the same procedure used in the narrow face, the offset distance for the wide face was also calculated.

Table 1. Narrow face thermocouple temperature comparison.

Distance Below Meniscus (mm)	3-D model	CON1D		CON1D with Offset	
	Temperature (°C)	Temperature (°C)	Difference (°C)	Temperature (°C)	Difference (°C)
115	186.6	165.4	-21.2	187.5	0.9
249	148.9	133.6	-15.3	150.0	1.1
383	135.7	122.5	-13.2	136.7	1.0
517	126.3	114.7	-11.6	127.4	1.1
651	129.8	118.0	-11.8	131.1	1.3
785	137.6	124.9	-12.7	139.0	1.4
919	142.9	129.6	-13.2	144.3	1.4

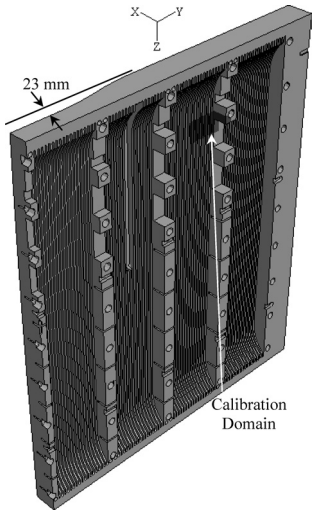

Fig. 8. Location of wide face calibration domain.

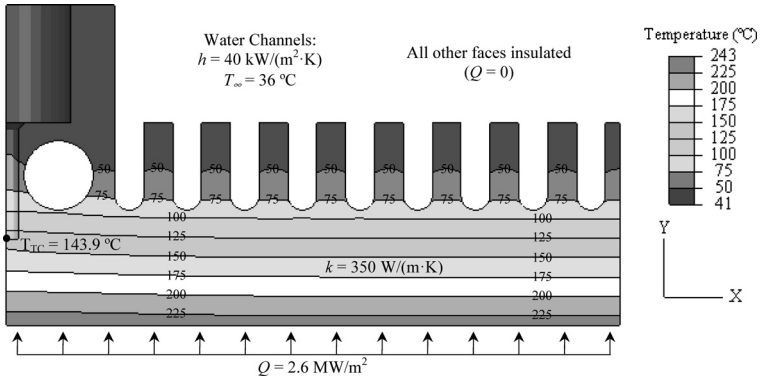

Fig. 9. Wide face calibration domain with input parameters.

Figure 8 shows a symmetric half of the wide face mould, and highlights the location of the calibration section. The boundary conditions and properties were maintained the same as in the narrow face. A top view of these conditions and the three-dimensional temperature distribution is plotted in **Fig. 9**.

The thermocouples in the real wide face are positioned 15 mm from the hot face. The offset was found to be 2.41 mm, meaning that the thermocouples in CON1D should be 2.41 mm closer to the hot face in order to produce accurate thermocouple predictions.

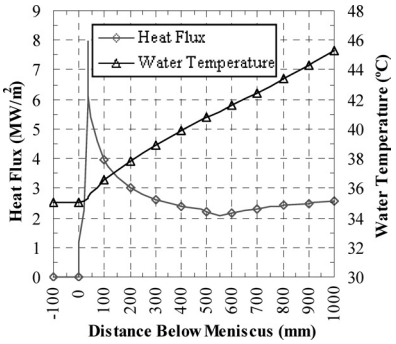

Fig. 10. CON1D output heat flux and water temperature profiles as input to ABAQUS.

4. Three-dimensional Mould Temperatures and CON1D Model Verification

Having calibrated the CON1D model by determining the offset distance, both the full three-dimensional model and CON1D simulation were run using realistic boundary conditions for the mould.

4.1. Narrow Face

One symmetric half of the entire three-dimensional narrow face geometry was analysed in ABAQUS, using the DFLUX and FILM user subroutines[12] to apply the shell-mould heat flux and cooling water temperature, respectively, as functions of distance down the mould, as given in **Fig. 10**. The thermal conductivity and water channel boundary conditions were not altered from the calibration model. This ABAQUS model used 468 583 quadratic tetrahedron elements and required 7.1 min (wall clock) to analyse.

Figure 11 shows the temperature contours from the three-dimensional model of the entire mould narrow face. Localized three-dimensional effects are observed near the peak heat flux region and at mould bottom. The cooler spot around the centre of the hot face corresponds to an inflection point in the heat flux curve. The highest temperatures occur at the small, filleted corners of the mould at the peak heat flux because those locations are furthest away from the water channels.

Figure 12 shows the three-dimensional hot face temperatures extracted along the mould centreline compared with the hot face temperatures from CON1D. The two models match very well (typically within 2°C) except around the areas with strong three-dimensional effects. Maximum errors are 9.2°C near the heat flux peak and 27°C at mould bottom, where the water slots end.

Figure 13 shows the temperature contours around the area of peak heat flux, highlighting the localized thermal

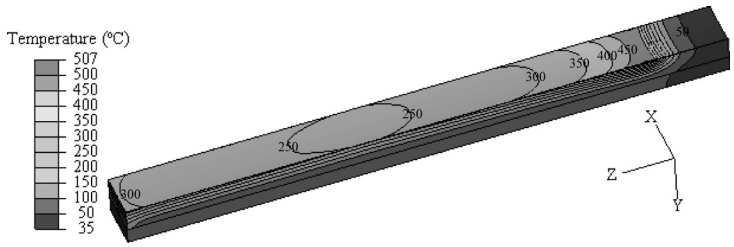

Fig. 11. Full three-dimensional model temperature results.

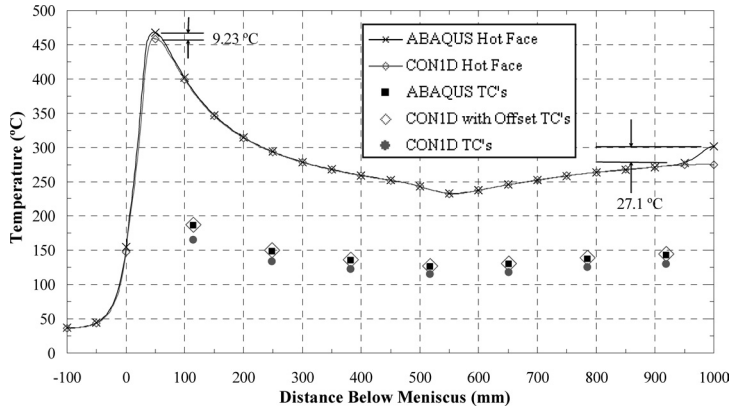

Fig. 12. Narrow hot face and thermocouple temperatures comparison between CON1D and ABAQUS.

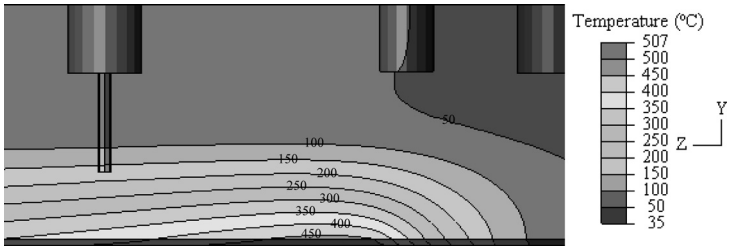

Fig. 13. Temperature contours around the peak heat flux.

Table 2. Wide face ABAQUS and CON1D comparison.

Parameter	ABAQUS	CON1D
Hot face temperatures	237.2 - 243 °C	237.4 °C
Cold face temperatures in the cooling channels: Point 1- bottom of curved channel root Point 2- first straight points after the curve	Point 1- 89.44 – 91.43 °C Point 2- 75.08 – 77.75 °C	81.4 °C
Temperature at the thermocouple location	143.9°C	143.90 °C (with offset)

effects at this location. Although the CON1D model is least accurate at the hot face at this location, its two-dimensional mould temperature calculation in the vertical slice allows it to achieve acceptable accuracy.

The temperatures predicted at all seven of the thermocouple locations in the mould compare closely with the offset CON1D values in Fig. 12. The topmost of the eight bolt holes does not have a thermocouple and the middle hole in Fig. 13 is for alignment. The results are tabulated in Table 1 and illustrated in Fig. 12. The temperatures match almost exactly (within 1.4°C or less), which is within the finite-element discretization error. This is a great improvement over the error of 12 to 21°C produced by CON1D without the offset. Lowering the location of the peak heat flux by 80 mm to the level of the first thermocouple (such that localised three-dimensional effects are at a maximum) and applying the offset method leaves an error of only −3.4°C at that thermocouple in CON1D.[14] Figure 12 also shows that the CON1D offset method is independent of heat flux, since the same offset was applied to all thermocouples. This means that a given mould geometry needs to be modelled in three dimensions only once prior to conducting parametric studies using CON1D.

4.2. Wide Face

In **Table 2**, ABAQUS and CON1D output results are compared along the mould perimeter in the calibration domain, 219 mm below the meniscus. The temperature at the cold face is tabulated at two points, and **Fig. 14** shows the temperature profile around the perimeter of a wide face water channel. As expected, point 1 is always hotter (around 90°C) than point 2 (around 76°C). The CON1D predicts temperature of the water slot root (cold face) to be 81.4°C, which lies in between these two values. Water slot tempera-

tures near the bolt hole are slightly higher than those near the symmetry plane.

These results show that CON1D can produce temperature predictions with the accuracy of a three-dimensional model in both the wide and narrow faces for any heat flux profile. In addition to its increased speed and ease-of-use, the CON1D model includes powerful additional calculations of the interfacial gap and solidifying shell. Thus, calibrating the CON1D model using the offset method to incorporate the three-dimensional ABAQUS results unleashes a powerful and accurate tool to study continuous casting phenomena.

5. Validation with Plant Data and Typical Results

After verifying that the CON1D model matches with the full three-dimensional model, the next important step is to validate CON1D results with plant data and to check the accuracy of the model under different casting conditions.

5.1. Database Comparison

A large database of plant data was compared with CON1D simulation results. The database contains more than 700 average values of heat flux, thermocouple temperatures, and mould powder consumption (measured with a load cell), recorded from the wide faces during stable casting periods. A stable casting period consists of at least 30 min of operation when the most important casting parameters, including casting speed and slab width, are approximately constant. These data were downloaded from the mould thermal monitoring (MTM) system and the level 2 control system of the caster that records all relevant data in real time.

The first comparison with plant data was done for the average mould heat flux (from the cooling water) for different casting speeds. The data were separated according to mould copper thickness into thick new plates (with 0 to 5 mm mould wear) and thin old plates (with 10 to 15 mm mould wear). The logarithmic curve-fit lines match with CON1D predictions, as shown in **Fig. 15**. This match is partly due to the effect of a thinner shell decreasing the thermal resistance at higher casting speed and thinner mould lowering the mould resistance, which both increase heat flux. The realistic input data, given in **Table 3**, allow CON1D to capture these effects. The match was improved by incorporating changes in the solid slag layer velocity, as discussed later. In addition to investigating mould temperatures, shell growth and interfacial phenomena, this calibrated and validated model enables extrapolation to predict behaviour at higher casting speeds.

5.2. Velocity Ratio between Solid Slag Layer and Steel Shell

In addition to heat, momentum, and force balances[5] a complete mass balance is performed by CON1D at each distance down the mould, to ensure that all three compo-

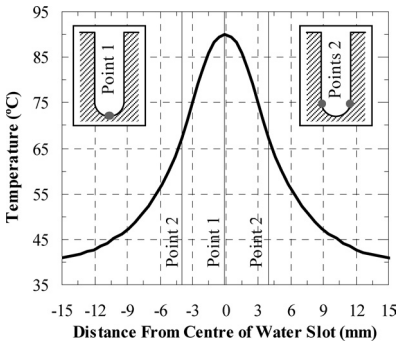

Fig. 14. Temperature profile around the perimeter of a wide face water channel.

Table 3. Simulation conditions.

Carbon Content, *C%*	0.045	%
Liquidus Temperature, T_{liq}	1531	°C
Solidus Temperature, T_{sol}	1509	°C
Steel Density, ρ_{steel}	7400	kg/m^2
Steel Emissivity, ε_{steel}	0.8	-
Initial Cooling Water Temperature, T_{water}	33	°C
Cooling Water Velocity, V_{water}	8.5	m/s
Mould Emissivity, ε_{mould}	0.5	-
Mould Slag Solidification Temp., T_{fsol}	1183	°C
Mould Slag Conductivity, k_{solid}, k_{liquid}	1.0, 1.5	W/(m·K)
Air Conductivity, k_{air}	0.06	W/(m·K)
Slag Layer/Mould Resistance, $r_{contact}$	9.5E-5	m^{2}K/W
Mould Powder Viscosity at 1300°C, μ_{1300}	0.9	Poise
Viscosity Temp.-dependence exponent, *n*	2.7	-
Slag Density, ρ_{slag}	2600	kg/m^3
Slag Absorption Factor, *a*	250	m^{-1}
Slag Refractive Index, *m*	1.667	-
Slag Emissivity, ε_{slag}	0.9	-
Pour Temperature, T_{pour}	1545	°C
Slab Geometry, width×thickness $W \times N$	1420×70	mm×mm
Nozzle Submergence Depth, d_{nozzle}	150	mm
Oscillation Mark Geometry, $d_{mark} \times w_{mark}$	0.08×1.5	mm×mm
Mould Oscillation Frequency, *freq*	325	cpm
Oscillation Stroke, *stroke*	6.0	mm

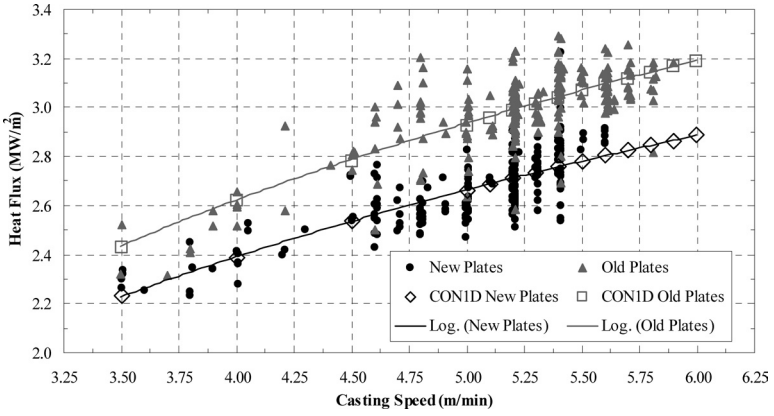

Fig. 15. CON1D mean heat flux compared to plant data.

nents of mould flux transport down the gap (oscillation marks, liquid movement, and solid movement) contribute properly to the total mould powder consumption.[11] The solid slag layer is assumed to move down the mould at a time-averaged velocity that varies with distance down the mould according to the behaviour of the liquid layer, interfacial friction, heat transfer, and other phenomena. This velocity, V_{flux}, ranges between zero (if the slag layer is attached to the mould) and the casting speed (if the slag layer is attached to the shell). The ratio between the solid slag speed and the casting speed must be input to the CON1D model. For a given powder consumption rate, this controls the time- and spatial-averages of the slag layer thickness, which greatly influences mould heat flux. This ratio is estimated from the following mass balance, assuming that liquid flux exiting the mould is negligible:

$$\frac{V_{\text{flux}}}{V_{\text{C}}} = \frac{Q_{\text{MP}}}{\rho d_{\text{slag}}} \quad \text{.....(2)}$$

Where V_{flux}: the velocity of the solid slag layer (m/min)
V_{C}: the casting speed (m/min)
Q_{MP}: the mould powder consumption (kg/m^2)
ρ: the mould slag density (kg/m^3)
d_{slag}: the slag layer thickness (m)

In practice, this velocity ratio varies with distance down the mould, which was characterized in this work to increase linearly between two values. At the meniscus, the ratio is zero, because the solid slag sticks to the mould wall and is relatively undisturbed due to the low friction associated with the liquid slag layer lubrication. At mould exit, Eq. (2) is used to estimate the solid flux velocity, based on the typical thickness of the solid slag layer that was measured at mould exit. After the shell temperature drops below the solidification temperature of the mould slag, the liquid slag layer runs out. Beyond this point, the increasing solid velocity ratio is accompanied by a decrease in thickness of the solid slag layer in order to maintain the mass balance.

Slag film fragments previously taken from the mould exit of the DSP caster ranged from 50 to 500 μm in thickness[15] and many of the fragments were found to be split into thinner mould-side and shell-side pieces. An average thickness of 200 μm was used as a first approximation in calculating the velocity ratio with Eq. (2). Further velocity ratios were found as a function of casting speed for both new and old mould plates, to match the average heat fluxes from the plant data. These two sets of ratios are plotted in **Fig. 16**, and compared with mould powder consumption. Mould powder consumption in the model is based on measurements in **Fig. 17** obtained in the DSP caster using a continuous measurement system equipped with load cells.

The velocity ratio has a strong correlation with the mould powder consumption, as given in Eq. (2). This relation also can be seen in Fig. 16, where both velocity-ratio curves drop with increasing casting speed in the same way as the mould powder consumption. This finding is logical because a higher casting speed increases both hot face temperature and shell surface temperature in the mould. This encourages a hotter, thicker liquid slag layer that extends further down the mould, which encourages the solid slag layer to remain more attached to the mould wall, producing a lower velocity. Furthermore, the higher hot face temperature tends to keep the mould slag above its glass transition temperature, making slag fracture less likely and thus lower average velocity ratio at higher casting speed.

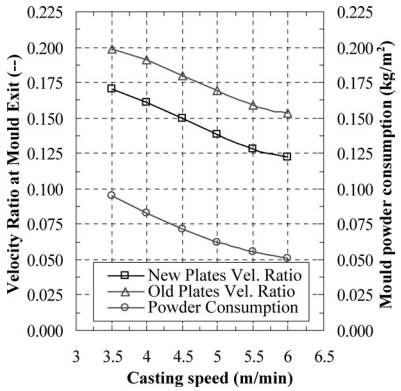

Fig. 16. Effect of casting speed on consumption and velocity ratios in new and old mould plates.

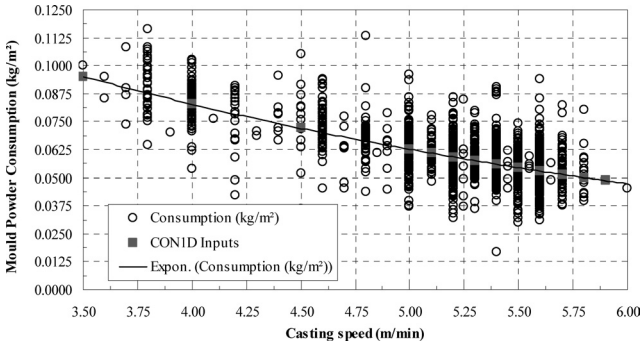

Fig. 17. Measured mould powder consumption compared with CON1D input values.

Mould heat flux varies with casting speed, velocity ratio and mould plate thickness. The CON1D results indicate that the velocity ratio itself varies with plate thickness. As older plates become thinner with wear, the mould hot face temperature is reduced, which has a similar effect to decreasing casting speed. Thus, the velocity ratio is expected to increase with old plates, as shown in Fig. 16. The actual speed of the moving solid slag layer is not easily measured. Thus, the application of calibrated and validated models such as CON1D is important to achieve the understanding of mould phenomena necessary to extrapolate plant data to new conditions and to solve product quality problems.

5.3. Temperature Validation

Plant data were obtained from a mould instrumented with forty thermocouples, as part of the standard MTM system to evaluate further the CON1D predictions. A period of 23 min of stable casting at a speed of 5.2 m/min and a width of 1 328 mm was chosen for this comparison, due to its stability in the thermocouples measurements. The meniscus level was measured to be about 100 mm below the top of the mould. Although the mould is capable of having a thermocouple in every bolt hole, the instrumented mould has only four rows of thermocouples. The first and fourth rows have 10 thermocouples, while the middle two rows have two thermocouples. The rows are 75, 200, 325, and 450 mm below the meniscus. Further details are provided elsewhere.[16] The 15 mm thermocouple depth below the hot

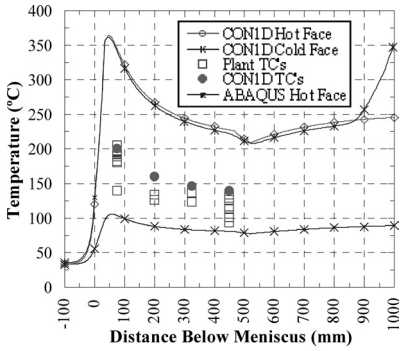

Fig. 18. Predicted thermocouple temperatures compared with plant data in the considered period.

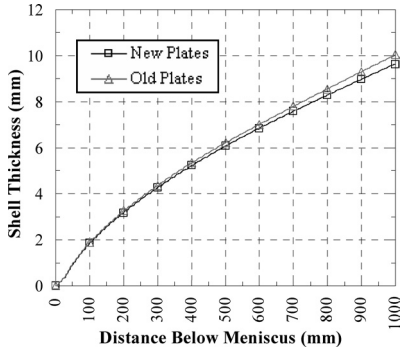

Fig. 19. Shell thickness profiles for new and old moulds.

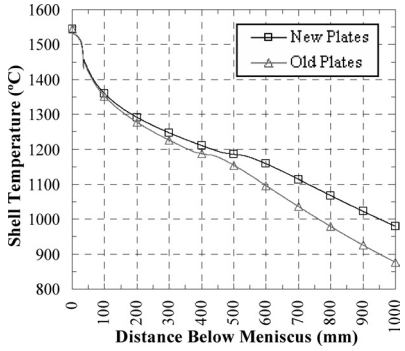

Fig. 20. Shell surface temperature profiles for new and old moulds.

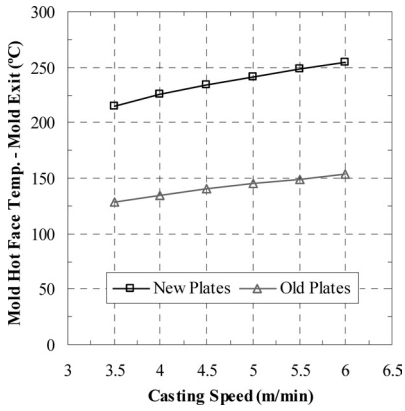

Fig. 21. Effect of casting speed on mould hot face temperature.

face was offset by 2.41 to 12.59 mm for CON1D.

The predicted hot face temperature profile, cold face (water slot root) temperature profile and thermocouple temperatures from CON1D are shown in **Fig. 18**. Hotface temperature from the 3-D ABAQUS wideface model matches CON1D, except near mould exit where the water slots run out. This figure also shows the average of the measured temperatures, which are slightly lower than predicted. This might be due to boiling in the water channels or minor contact problems, both of which result in a lower mould temperature. Scale formation in the water channels would cause the mould temperature to increase, providing another explanation for the variability in the measurements.

5.4. Solidification Model Results

Having validated the CON1D model capability to predict heat flux and mould temperature distribution down the mould, this modelling tool was applied to predict solidification and temperature evolution of the steel shell, and the behaviour of the mould flux layers in the interfacial gap. Typical results are presented in **Fig. 19** and **Fig. 20** for the conditions in Table 3, comparing the wide face of new and old moulds at 5.5 m/min casting speed.

Shell thickness increases down the mould at a decreasing rate, as the solid resistance increases. This contributes to lowering the heat flux across the interfacial gap. Shell thickness and heat flux are both lower for the new mould because the thicker mould provides additional thermal resistance, though he effect is very slight. The shell surface temperature also drops with distance down the mould, with variations that depend on the local heat flux. The lower surface temperature for old plates is due to the higher heat flux. The changes in slag layer thickness down the mould, which are governed by the changing solid velocity ratio, greatly affect all of these results. Further details on application of the CON1D model under realistic conditions are given elsewhere.[5)]

6. Parametric Study

The verified, calibrated, and validated CON1D model is being applied to investigate a range of mould thermal phenomena, including high-speed casting, mould powder properties, scale formation in the water channels and breakout prediction. The effect of mould plate thickness and casting speed on interfacial gap phenomena are investigated here. In each simulation, the velocity ratio and mould powder consumption were taken as functions of casting speed according to Fig. 16.

The effects of casting speed and mould plate thickness on various parameters at mould exit are shown in **Figs. 21–24**. Increasing casting speed naturally increases the mould hot face temperature and decreases the shell thickness. This causes the slab surface temperature to increase, although the increased heat flux with increasing casting speed tends to counter this trend. Slag layer thickness decreases with casting speed, owing to the smaller slag consumption rate, but the opposing effect of lower solid slag velocity ratio tends to lessen this trend.

Decreasing the mould plate thickness (as the plates become older) decreases the hot face temperature as expected. This increases the solid slag layer velocity (Fig. 16), which produces a thinner slag layer, as shown in Fig. 24. Com-

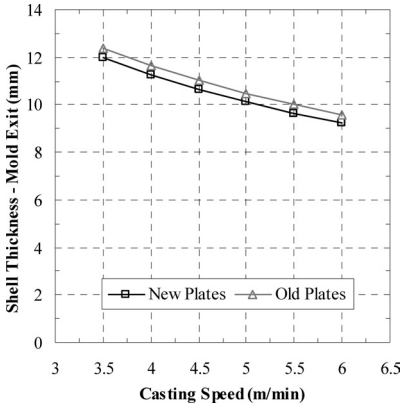

Fig. 22. Effect of casting speed on shell thickness.

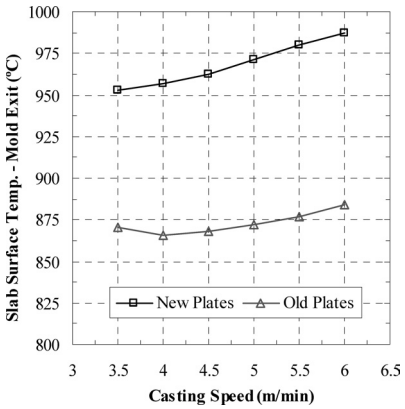

Fig. 23. Effect of casting speed on slab surface temperature.

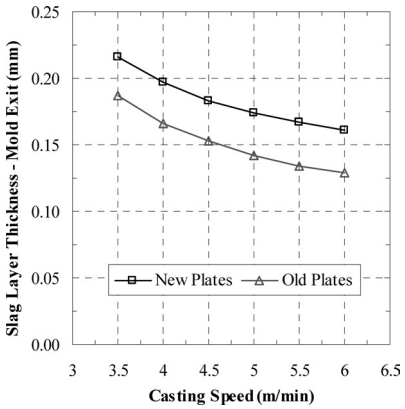

Fig. 24. Effect of casting speed on slag layer thickness.

bined with the smaller resistance of the thinner mould plate, this increases the heat flux. This causes the shell thickness to increase slightly and slab surface temperature to decrease. These effects might be compensated by adding a thicker mould coating layer, or by carefully decreasing the water slot velocity as the moulds age and become thinner.

7. Conclusions

This work summarizes the development of an accurate computational tool for modelling heat transfer in the thin-slab continuous casting mould at the Corus DSP. Work towards this end includes model verification with a complete thermal three-dimensional analysis of the entire complex mould geometry, model calibration using the offset method to match thermocouple measurements and model validation with over 700 sets of plant data from an instrumented mould. The CON1D model is then applied together with plant measurements to gain new insights into the effects of casting speed and mould plate thickness on mould heat transfer. Project findings include:

(1) Increasing casting speed causes a thinner solidified steel shell, higher heat flux, higher mould hot face temperature, a thinner slag layer and lower solid slag layer velocity.

(2) Increasing mould plate thickness increases hot face temperature, lowers solid slag layer velocity, increases slag layer thickness, and lowers mould heat flux.

The CON1D model is being applied to gain further insight into continuous casting of thin slabs, including the extrapolation of model predictions of heat transfer and interfacial phenomena to higher casting speed and the optimisation of mould taper, mould distortion, and funnel design.

Acknowledgements

The authors wish to thank the member companies of the Continuous Casting Consortium and the National Science Foundation (Grant # 05-00453) for support of this work, the National Center for Supercomputing Applications (NCSA) for computational resources, and personnel at Corus DSP for plant data and support.

REFERENCES

1) J. K. Park, B. G. Thomas, I. V. Samarasekera and U. S. Yoon: *Metall. Mater. Trans. B*, **33B** (2002), No. 3, 425.
2) J. K. Park, B. G. Thomas, I. V. Samarasekera and U. S. Yoon: *Metall. Mater. Trans. B*, **33B** (2002), No. 3, 437.
3) T. G. O'Connor and J. A. Dantzig: *Metall. Mater. Trans. B*, **25B** (1994), No. 3, 443.
4) J. W. Shaver: Masters Thesis, University of British Columbia, (2002).
5) Y. Meng and B. G. Thomas: *Metall. Mater. Trans. B*, **34B** (2003), No. 5, 707.
6) Y. Meng and B. G. Thomas: *ISIJ Int.*, **46** (2006), No. 5, 660.
7) H. Nam, H.-S. Park and J. K. Yoon: *ISIJ Int.*, **40** (2000), No. 9, 886.
8) Y. Xie, H. Yu, X. Ruan, B. Wang and Y. Ma: *Int. J. Adv. Manuf. Technol.*, **30** (2006), 645.
9) X. S. Zheng, M. H. Sha and J. Z. Jin: *Acta Metall. Sin. (Engl. Lett.)*, **19** (2006), No. 3, 176.
10) C. Chow, I. V. Samarasekera, B. N. Walker and G. Lockhart: *Ironmaking Steelmaking*, **29** (2002), No. 1, 61.
11) Y. Meng and B. G. Thomas: *Metall. Mater. Trans. B*, **34B** (2003), No. 5, 685.
12) ABAQUS 6.6-1. 2006, Dassault Simulia, Inc., 166 Valley Street, Providence, RI, USA 02909-2499, (2006).
13) M. M. Langeneckert: Masters Thesis, University of Illinois, (2001).
14) L. C. Hibbeler and B. G. Thomas: Continuous Casting Consortium Report 200701, (2007).
15) J. A. Kromhout, S. Melzer, E. W. Zinngrebe, A. A. Kamperman and R. Boom: *Steel Research Int.*, **79** (2008), No. 2, 143.
16) B. Santillana, B. G. Thomas, A. Hamoen, L. C. Hibbeler, A. A. Kamperman, W. van der Knoop: Proc. of AISTech 2007 Steelmaking Conf., No. 2, AIST, Warrendale, PA, (2007), 25.